Sensor and Simulation Notes

Note 420

May 1998

NUMERICAL ANALYSES OF TEM HORN ARRAYS

Daniel T. McGrath, LtCol, USAF

Air Force Research Laboratory
Directed Energy Diretorate
Kirtland AFB, NM

ABSTRACT

A numerical model is used to assess the wideband radiating and receiving properties of TEM horn radiators in large arrays. Configurations without and with a ground plane to prevent back lobe radiation, and linear and exponential-flare plate profiles were studied. An exponential flare profile in the E plane reduces the periodic impedance variation with frequency from which the open-backed linear flare array suffers. When a ground plane is introduced behind a TEM horn array, it prevents low frequency radiation or reception. In addition, there may a scan blindness due to a trapped wave mode between the horn plates and ground plane. This blindness may be prevented (at the expense of a loss in low frequency performance) by making the horns shallower, with a larger interior angle. Within these guidelines it is possible to create an array with over 150% instantaneous bandwidth that can scan to ±60° in the E plane.

1. INTRODUCTION

It is well known that array antennas would have important advantages as sources of high-power fast-risetime transients. Among these are the ability to achieve higher radiated power than with a single source and a capability for electronic beam steering. The general concept of using interconnected TEM (transverse electromagnetic) horns in arrays, as illustrated in Figure 1, has been available for many years [1], but has yet to be exploited in practice for planar arrays with large numbers of elements.

Earlier work explored the properties of planar bicone (PBC) arrays, establishing the limits on their bandwidth and scanning performance due to inter-element mutual coupling [2]. It also determined the guidelines for modeling these types of antennas using a finite element code. This work was later extended to open-backed TEM horns, again showing that the computer code gives accurate results for input impedance and element gain [3].

An essential limitation of the open-backed arrays, whether planar bicones or TEM horns, is that they have significant back-lobe radiation. In the case of the PBC element, the front and back lobes have equal magnitude. Even with very small half angles, the TEM horn arrays have over 10% back lobe radiation. To suppress the back lobes, it is necessary to introduce a ground plane behind the array. (There are concepts for using resistor lattices to absorb the backwards radiation, but they require a significant air volume behind the array, which is undesirable.) This report shows the limits on performance that are caused by the addition of a ground plane located at the horn apex, very close to the feed point. It limits the bandwidth to the general range of 100% to 150%, because a shallow element with a large half angle has poorer low frequency performance, while a deep element with a small half angle will permit a "scan blindness" due the excitation of a parallel-plate-like slow-wave mode between the horn structure and the ground plane. As a prelude to this discussion, the earlier results for PBC arrays and TEM arrays without ground planes are summarized. The behavior of dual-polarized TEM horns in the array environment is also discussed.

2. ANALYSIS APPROACH

Any calculation of the element gain and input impedance of antennas in closely-spaced arrays must rigorously account for the effects of mutual coupling between elements. The most practical methods for analysis of mutual coupling effects begin with an assumption that the arrays are large enough so that each individual element sees the same environment. In other words, edge effects do not appreciably change the performance characteristics of the individual radiating elements. When that is the case, an infinite array assumption may be used to restrict the analysis to a single array "unit cell."

In the periodic hybrid finite element approach, presented in [4] and [5], the unit cell is subdivided into volume elements (tetrahedra) over which expansion functions for the electric field are defined. Figure 2 shows an example "mesh" for a TEM horn element, with the cells in the horn interior blanked to show the shape of the conductors (shaded). The model may include resistive wires to emulate point loads. The mesh edge length is typically smaller near the feed point so that the solution can accurately capture the field behavior in that region, where the spatial variation of electric field with position is large.

In this work, the field expansion functions are linear, edge-based vector elements. The finite element region is terminated at planes both above and below (on the $+z$ and $-z$ sides, respectively) the physical structure. At those planes, a periodic radiation boundary condition is imposed. That condition, based on an integral equation, provides a reflectionless absorbing boundary for outgoing waves at all angles. In addition, periodicity conditions are enforced at the unit cell side walls, effectively wrapping opposing faces in x and y onto each other with a phase shift appropriate to the array scan angle. The formulation leads to a system of equations that must be constructed and solved separately for each scan angle and frequency.

In all of the cases discussed below, the mesh edge length was equal to or smaller

than $\lambda/10$ at the highest frequency for which calculations were required, and still finer in the vicinity of the feed points. The matrix solver used the biconjugate gradient method [6] with a residual error threshold of $1x10^{-5}$. All Floquet modes with orders from -10 to 10 were used in calculating the matrix terms associated with the periodic radiation boundaries (a total of 441 modes). These mesh granularities, mode limits, and residual thresholds were confirmed to give convergence of the received current through a load at the feed point to within 0.1% [2].

2. PLANAR BICONE ARRAYS

The planar bicone (PBC) is a limiting case of the TEM horn, in which the half angle is $\beta=180°$. The PBC array, illustrated in Figure 3, is capable of radiating waveforms with very low frequency components because the sources are connected in series. The low frequency radiation is limited only by that frequency at which the entire (finite) array is one half wavelength across.

PBC arrays are not adequate for most applications because they are bidirectional, radiating equally into each half space at all frequencies. However, they are an interesting starting point for analysis because of the fact that when the lattice is square ($d_x=d_y$) it is "self-complementary." That is, a rotation of 90° about any feed point results in the complementary structure, with conductor replacing free space and vice-versa. Consequently, its input impedance is $\eta_0/2$, independent of frequency [7], where $\eta_0=120\pi\ \Omega$. This property has been confirmed for frequencies up to the half-wavelength lattice dimensions by measurements of a line source array in parallel plate waveguide [8]. One reason for studying the PBC array is to assess the effects of non-ideal feed geometries. Figure 3b shows a configuration that gave the best results in the earlier study [2].

2.1. Input Impedance

Computed values of Z_{in} are shown in Figure 4. Note that f_0 is that frequency at which the lattice dimensions are exactly one wavelength, i.e. $d_x=d_y=\lambda_0$. When frequency increases through f_0, eight grating lobes enter visible space, four in each half space, causing an abrupt discontinuity in Z_{in}. When the frequency increases through $\sqrt{2}f_0$, a second set of grating lobes becomes visible, causing another discontinuity. Notwithstanding the presence of grating lobes, the input impedance remains near the expected value of $60\pi\ \Omega$, confirming its self-complementary property.

2.2. Frequency Response

When the planar bicone array is used as a transmitter with sources in phase, for frequencies up to f_0, it radiates half of its power in each direction normal to the array. Similarly, when receiving, one half the power in a broadside-incidence plane wave will be absorbed by the array when the feed points are loaded by $60\pi\ \Omega$ impedance. Figure 5 shows the received, forward scatter and back scatter power for the array element design of Figure 4b under those conditions of broadside incidence and $\eta_0/2$ load impedance. Within the grating-lobe free region, the received power is very nearly constant, which is a consequence of the frequency-independent, self-complementary property. However, as frequency increases through f_0, the form of the current induced on the bicone plates by the incident wave changes form, and very nearly all of the incident power reradiates, with very little being received by the array.

Figure 5 also shows the received power for an array with disconnected elements, having an air gap $\lambda_0/10$ wide between adjacent elements in the E plane (y-z). It is clear from this result that, as expected from [1] and [9], the interconnection between elements is essential for receiving or radiating low frequency components of transient waveforms.

Representative calculations of received power for off-broadside incidence are shown in Figure 6. For 30° and 60° incidence, the received power remains nearly constant at low frequencies, but drops sharply when the first grating lobes become visible at the frequency $f_{GL}=f_0/(1+\sin\theta_0)$, where θ_0 is the angle of incidence (measured from the -z axis). The frequency response magnitude again drops to nearly zero at f_0. Note that for a finite array, the low frequency response will differ from that shown in Figure 6. It will roll off sharply below that frequency at which the array length is one half wavelength in the direction of its polarization.

The importance of the results in Figures 5 and 6 is that although the PBC array exhibits frequency-independent input impedance properties, it is only useful up to the grating lobe limiting frequency f_{GL}. Although the input impedance remains acceptably near $\eta_0/2$ above that frequency, most of the radiated power ceases to go into the main beam, instead coupling primarily into the grating lobes.

3. OPEN-BACKED TEM HORN ARRAYS

3.1. Input Impedance

The input impedance for an isolated TEM horn may be directly calculated using stereographic and conformal mapping [10]. In the high frequency limit, this is also the impedance seen by an array element. For the square lattice dimensions, those limits are $.493\eta_0$ for $\beta=120°$, and $.481\eta_0$ for $\beta=60°$. In the low frequency limit, at broadside scan, the array element's input impedance is identical to that of a PBC array with the same lattice dimensions, i.e., $\eta_0/2$. In the intermediate frequency range, however, it is necessary to rely on either calculations or measurements to find Z_{in}.

The feed geometry used is similar to Figure 3b when viewed from the +z axis. The lattice is square with $d_x=d_y=\lambda_0$. Figure 7 compares Z_{in} vs. frequency for the $\beta=120°$ and

β=60° TEM horn elements and the PBC element at broadside scan.

Figure 8 shows the input impedance for four cases, with β=120° and β=60°, for scanning in the E and H planes. Each graph shows results for scanning to 30° and 60°. Note that the low frequency limit for input impedance when scanning to the angle θ_0 is $.5\eta_0\cos(\theta_0)$ or $.5\eta_0\sec(\theta_0)$ for scanning in the E and H planes, respectively. Both arrays perform better scanning in the E plane. The β=60° horn is more limited in its scanning ability, having large variations in Z_{in} vs. frequency when scanned away from broadside.

In each case in Figure 8, observe that at the highest frequencies calculated, the input impedance is the same, depending only on the flare angle, and not on the scan angle or scan plane. This confirms the proposition that the high frequency limit on Z_{in} depends only on the element's flare angle and aperture dimensions.

3.2. Frequency Response

To compute the array frequency response, the receiving case was simulated, using a load impedance of $\eta_0/2$ at the horn feed points. Figure 9 shows the receiving frequency response for the three TEM horns, as well as for the planar bicone. As expected, the smaller horn angles provide directionality: on receive, more of the incident power couples into the loads with less being reradiated. However, the frequency response magnitude is less uniform, exhibiting oscillations with increasing frequency. For the transmitting case, by reciprocity, the radiated power in the $+z$ direction is the difference between unity and the values in Figure 9. The peaks in the frequency response magnitude coincide with those frequencies at which the horn length is an integer multiple of one half wavelength.

Figure 10 shows the frequency response for the β=120° horn for a plane wave incident from 30° in both the E and H planes. In each case, the response drops dramatically at the angle when the first grating lobes become visible, then drops to nearly zero at f_0, just as in the planar bicone case. The responses are somewhat different near the first

grating lobe onset ($.65f_0$) because, in the E plane, the source couples into a TM Floquet mode, whose endfire admittance is infinite, decreasing as it moves into visible space [11:41-42]. When scanning in the H plane, the source couples into a TE Floquet mode, whose admittance is zero at endfire, increasing as it moves into visible space.

The results shown in Figures 9 and 10 indicate that there is an advantage to using the TEM horn element to improve directionality in the frequency range below f_0. However, their operation must still be restricted to the grating-lobe-free range of frequency and scan angle. For an ultrawideband transmitter, this means that the array lattice spacing must be chosen so that f_0 is equal to or above the highest frequencies that the sources generate. If that condition is not met, the energy above f_{GL} will not radiate in the intended direction.

Figures 11 and 12 show the received power and phase for, respectively $\beta=120°$ and $\beta=60°$, for scanning to various angles in the H plane. The phase is referenced to the center of the load. Within the grating-lobe free range of angle and frequency, the variation of power with frequency is within 3 dB for any particular scan angle, up to the onset of the first grating lobes. The variation in phase is worse for the $\beta=60°$ element. Consequently, either element could be used to radiate and receive transients from off-broadside angles using time-delay steering, although the $\beta=60°$ horn is more dispersive, implying a tradeoff between directionality and minimum-achievable rise time.

4. EXPONENTIAL FLARE TEM HORN

Figure 13 shows a comparison between TEM horns with linear and exponential flare shapes. The flare shape for the latter is one commonly used for flared notch antennas [12] given by

$$w(z) = w_0 \exp\left\{\frac{z}{\ell} \ln\left(\frac{w_m}{w_0}\right)\right\} \tag{1}$$

where w_0 is the width between plates at the feed point, w_m is the width at the mouth, and ℓ is the overall length. The two models have a 2:1 aspect ratio in order to provide a lower input impedance. Asymptotic formulas predict about 118 Ω for this horn aspect ratio [10] in the high frequency limit.

In the CAD model, the flare is not smooth, but is approximated by 5 flat sections as illustrated in Figure 14a. The first four, going in from the horn mouth, are 20% of the unit cell length in z, and the last is 10%, of the length, ending 10% away from the $+z$ side, where its width w_0 is 10% of d_y. From that point, the plates follow the same contour as the linear-flare horn, tapering down the feed point as shown in Figure 14b. The feed geometry for the linear-flare horn is the same.

The computed input impedance for these two cases is shown in Figure 15 for the case in which the unit cell is λ_0 long in the z direction. This corresponds to a horn angle of β=28°. As expected, the input impedance for both is approximately 30π Ω in the low frequency limit ($.5\ \eta_0 \cdot d_y/d_x$). At the higher frequencies it appears to be approaching 105Ω, although the calculations do not go high enough in frequency to establish it with certainty.

It is apparent from Figure 15 that the exponential flare has a much more stable input impedance as a function of frequency, as well as lower reactance. The consequence, in terms of ultrawideband radiation, is the exponential-flare array will have a flatter frequency response.

5. GROUND PLANE EFFECTS

The introduction of a ground plane behind the horn apices is expected to have two important consequences: (1) it will suppress low frequency radiation (undesirable); and (2) it will prevent back lobe radiation (desirable). It also turns out, as will be shown, that it can introduce a "scan blindness," a continuum of frequency-scan angle combinations that will result in no radiated power (very undesirable). This blindness can be suppressed by making

the horn flare angle larger, and hence making the structure shallower, but at the cost of making the low frequency performance worse [13]. Nonetheless, it is possible to construct TEM horn arrays that have greater than 100% *signal* or *instantaneous* bandwidth, over which the gain is within 3 dB of the maximum possible with the phase within 30° of linear.

The following simulations used the same geometries as shown in Figure 13. The only difference is that the $+z$ face is now a ground plane. The sources or loads are located L/10 away from the ground plane. Calculations were performed using lengths, L, of $.5\lambda_0$ (β=53°), $.75\lambda_0$ (β=37°), and λ_0 (β=28°).

5.1. Input Impedance

Figure 16 is, again, a comparison of Z_{in} for the linear and exponential flare horns, but this time with a ground plane (broadside incidence). As expected, the impedance drops to zero in the low frequency limit. Both geometries have an abrupt impedance discontinuity near $.6 f_0$, which is the scan blindness alluded to above, where the real part drops to zero.

Unlike the open-backed horn arrays, the exponential flare does not give a smoother Z_{in} vs. frequency than the linear flare when there is a ground plane.

Figures 17 and 18 show results for different flare lengths. Note that with decreasing flare length (shallower horns) the blindness moves up in frequency, and with $L=.5\lambda_0$ it has moved above f_0. This suggests that the most practical way to avoid it is to make L small. However, note that in doing so, the low frequency cutoff moves higher. Hence, there is a tradeoff between avoiding the blindness and preserving low frequency response.

The input impedances for the two horn arrays are considerably different in the "passband," between the low-frequency rolloff and the scan blindness--100 to 150 Ohms for the linear flare, and 50 to 100 Ohms for the exponential flare. Consequently, the following results for frequency response use 105 Ω for the linear flare and 75 Ω for the exponential flare.

5.2. Frequency Response

As before, the array frequency response is calculated in the receiving mode, with an incident plane wave from the -*z* half-space. The element is terminated with a resistive wire located at the feed point. The following graphs include both the magnitude and phase of the received current through the load. A constant phase slope has been subtracted from the phase to reference it to the load's location.

Figures 19 and 20 are for broadside incidence, comparing results for three different flare lengths. (Note: the frequency sampling was not as fine for these plots as it was for Figures 17 and 18, which gives the erroneous appearance that the blindness is incomplete.) The case with $L=.5\lambda_0$ is especially interesting: The half-power bandwidth is 150% for the exponential flare. Over that same band, the phase is flat to within ±20°. The linear flare's bandwidth is only slightly lower. This indicates that TEM horn arrays with ground planes are capable of transient radiation, provided that the waveform's content is not predominantly low frequency. For example, if f_0 is 2 GHz, then the exponential flare horn array will successfully radiate signal components as low as 300 MHz.

Figures 21 and 22 are for $L=.5\lambda_0$, and three different incidence angles in the E plane (y-z plane). Since the E plane spacing is $.5\lambda_0$, scanning in that plane will not generate grating lobes. Evidently, the blindness that is not evident at broadside becomes visible at 30° scan, then disappears at 60° scan. Other than that single feature, the exponential flare horn array maintains its bandwidth when scanning, with only a slight bandwidth loss on the low end at 60° scan. The same is not true of the linear flare array--at 60° scan the band center apparently shifts to a higher frequency, and the low frequency cutoff nearly doubles in frequency compared to broadside scan. This demonstrates that the exponential flare shape is very beneficial for a scanned array.

6. CONCLUSIONS

The impedance and scanning properties of TEM horn arrays have been assessed numerically. The limiting case, the planar bicone, was shown to have the frequency-independent property of a self-complementary antenna, making it a useful case for establishing the effects of feed region geometry. Although it radiates bidirectionally, it has the interesting property that its frequency response in the array environment is absolutely flat up to the grating lobe onset limit.

TEM horn arrays are more unidirectional, but as a consequence suffer an oscillatory variation in the input impedance with frequency. An exponential flare profile in the E plane reduces that impedance variation. Elements of TEM horn arrays, as well as those of planar bicone arrays, must be directly connected at the unit cell boundaries in the E plane to be able to radiate low frequencies.

When a ground plane is introduced behind a TEM horn array, it prevents low frequency radiation or reception. The low frequency cutoff is approximately $.067/L$ for the exponential flare and $.1/L$ for the linear flare, where L is the depth between the horn mouths and the ground plane. In addition, there may a scan blindness due to a trapped wave mode between the horn plates and ground plane. This blindness may be prevented (at the expense of a loss in low frequency performance) by making the horns shallower, with a larger interior angle. Within these guidelines it is possible to create a scanning array with over 150% instantaneous bandwidth that can scan to $\pm 60°$ in the E plane.

ACKNOWLEDGEMENTS

This work was supported in part by the Air Force Office of Scientific Research. The calculations were performed using resources of the Aeronautical Systems Center (ASC) and Waterways Experiment Station (CEWES) Major Shared Resource Centers and Maui High Performance Computing Center.

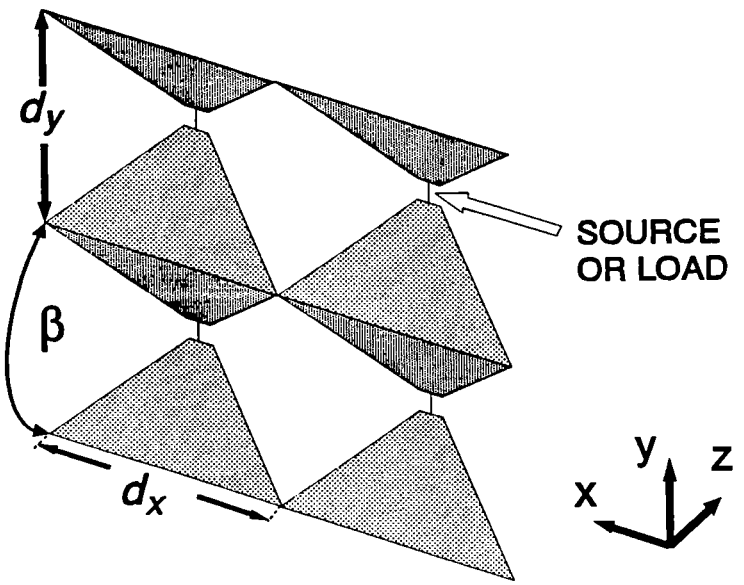

Figure 1. TEM Horn Array Geometry.

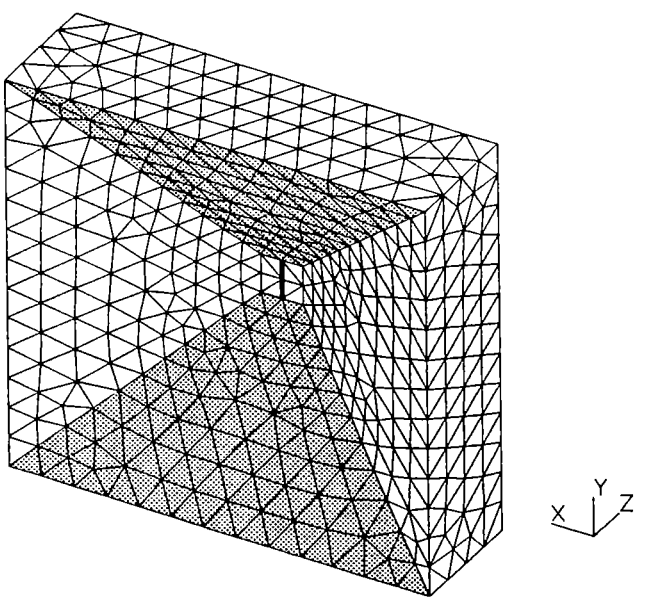

Figure 2. Typical Finite Element Representation of Array Unit Cell (Mesh cells in horn interior removed).

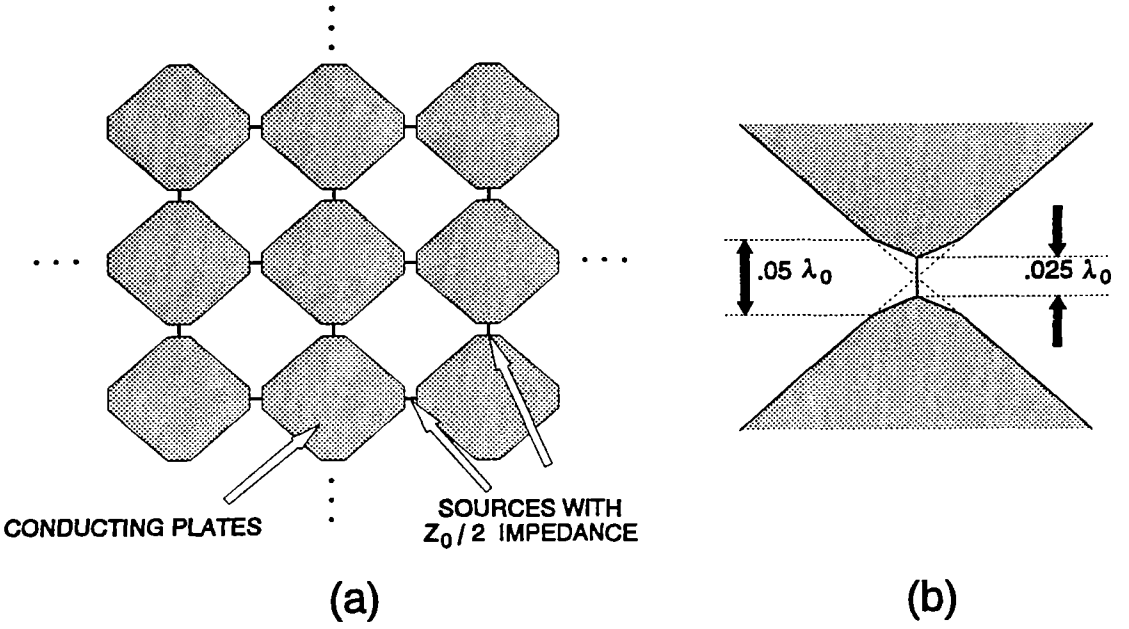

Figure 3. Planar Bicone Array: (a) Geometry; (b) Feed Region Detail

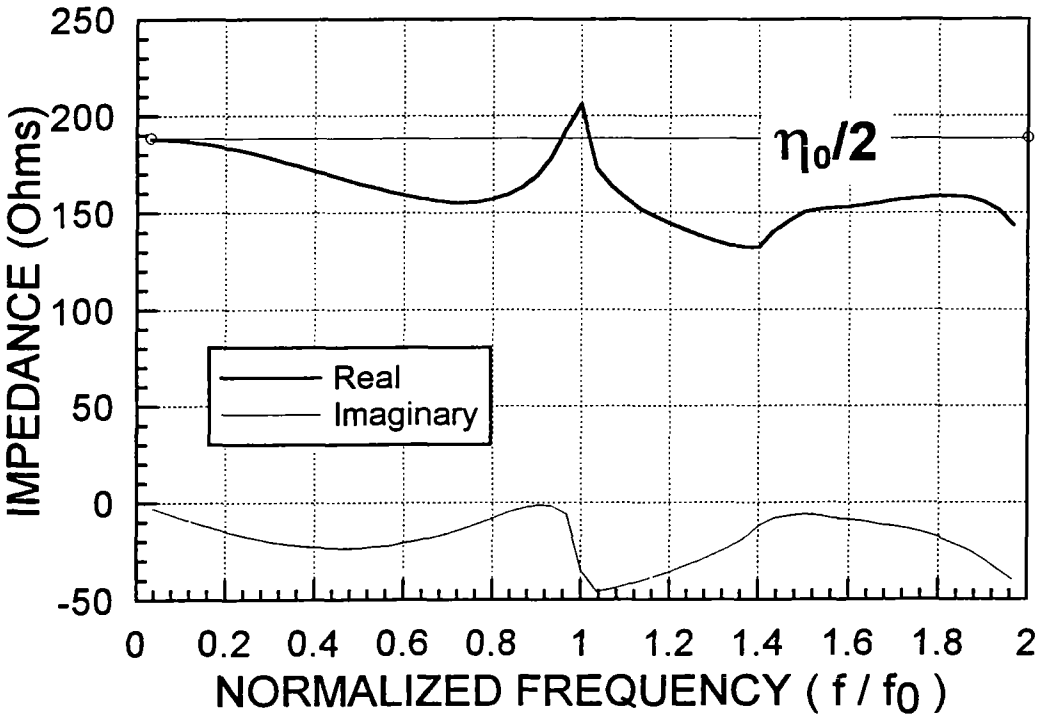

Figure 4. Input Impedance vs. Frequency for Planar Bicone Array with Square Lattice

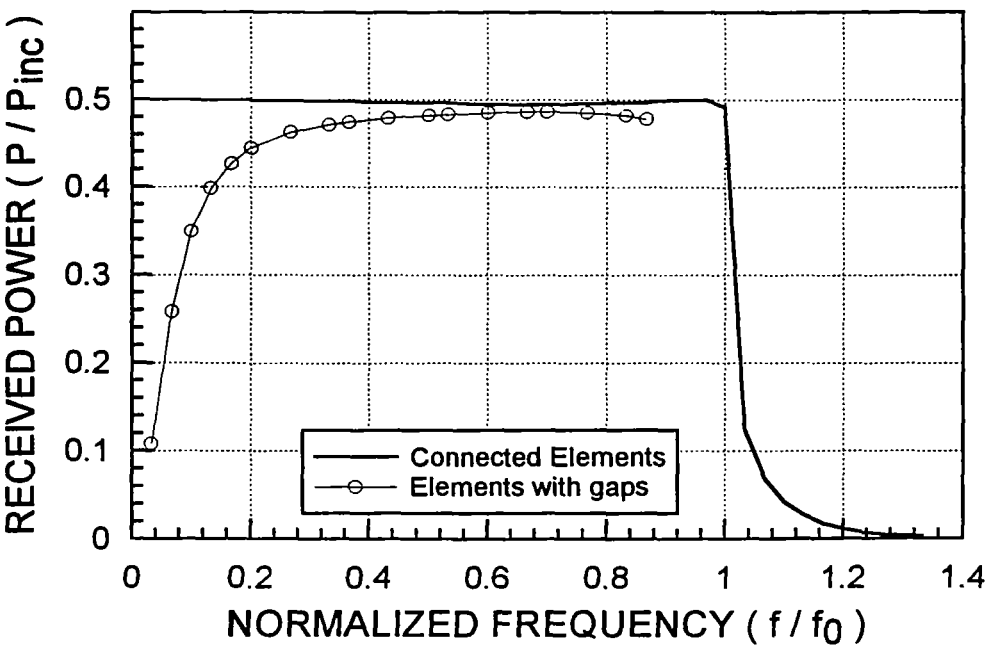

Figure 5. Received Power (Element Gain) for Planar Bicone Array with Connected Disconnected Elements, Broadside Incidence

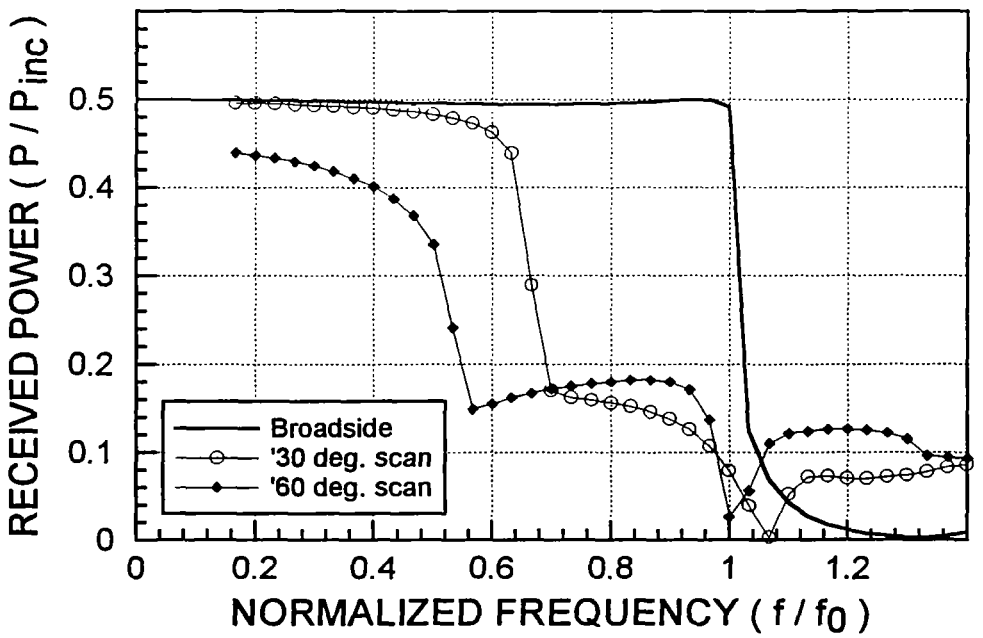

Figure 6. Planar Bicone Array Frequency Response with H Plane Scanning

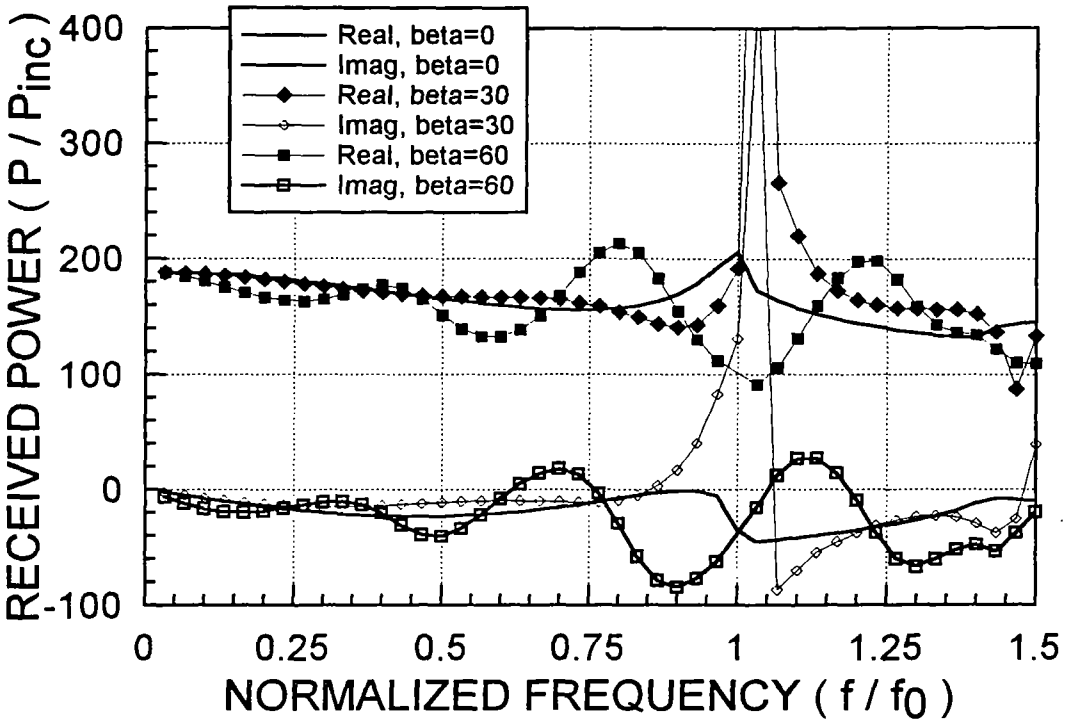

Figure 7. Input Impedance vs. Frequency at Broadside Incidence for β=60°, β=120° TEM Horn and Planar Bicone Arrays

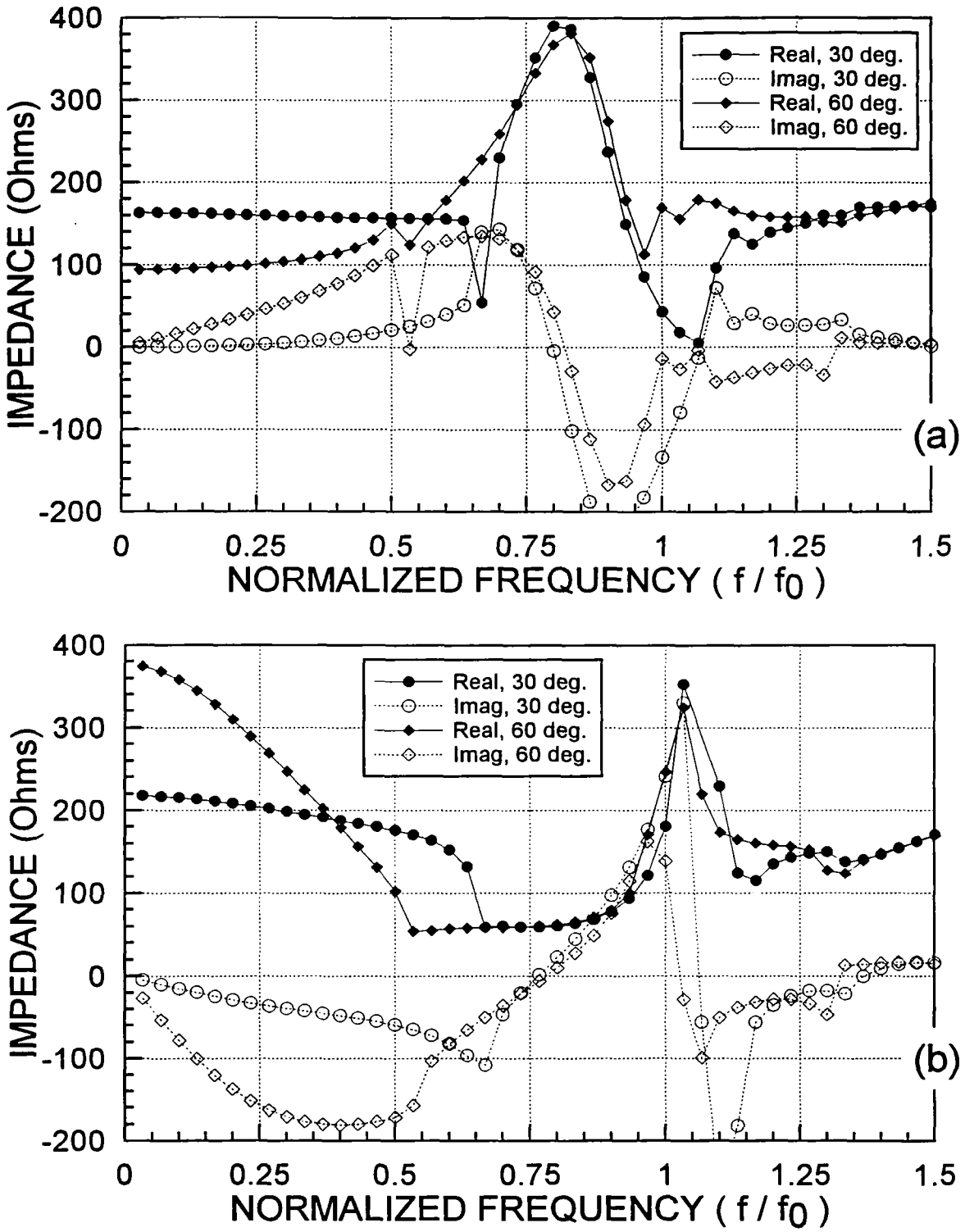

Figure 8. Input Impedance for θ=30° and θ=60° Scan: (a) β=120°, E Plane; (b) β=120°, H Plane; (c) β=60°, E Plane; and (d) β=60°, H Plane.

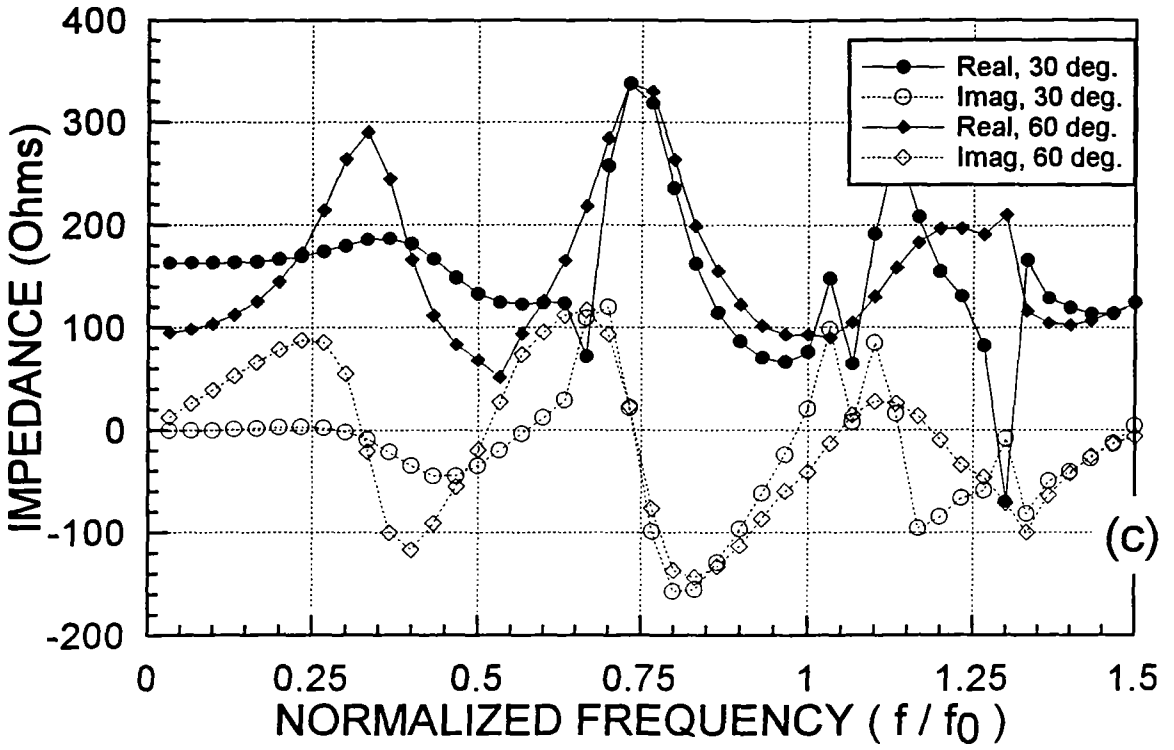

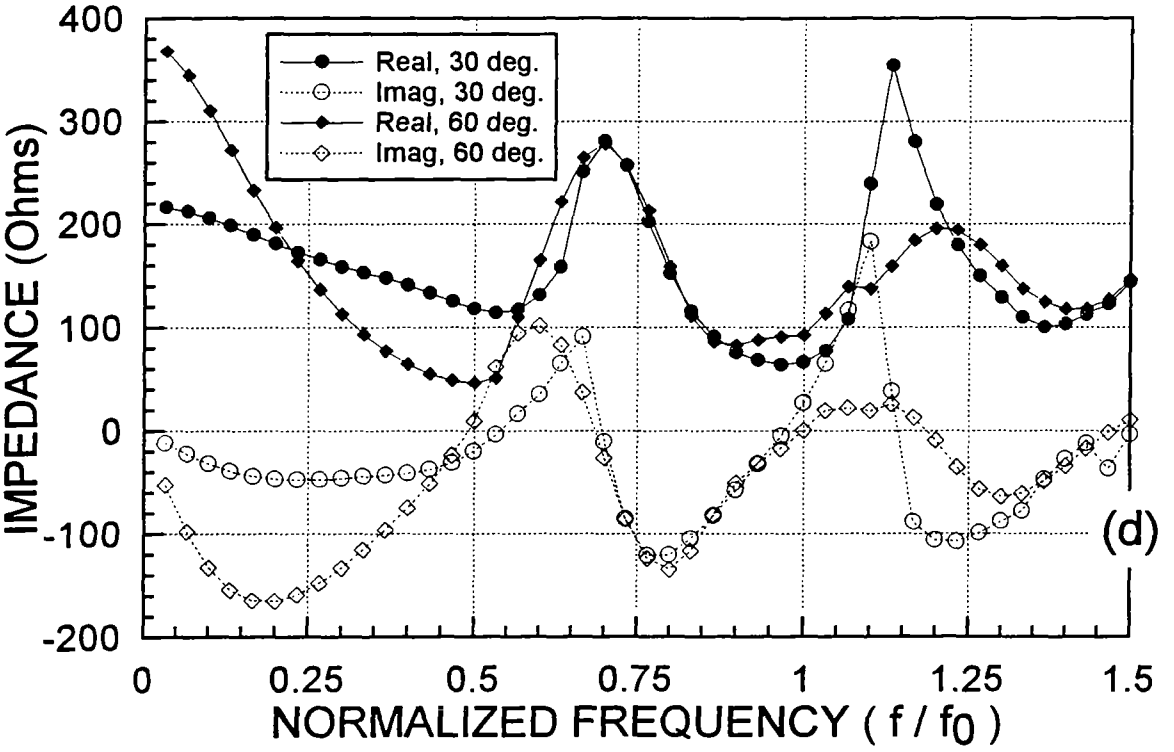

Figure 8 (cont.) Input Impedance for θ=30° and θ=60° Scan: (a) β=120°, E Plane; (b) β=120°, H Plane; (c) β=60°, E Plane; and (d) β=60°, H Plane.

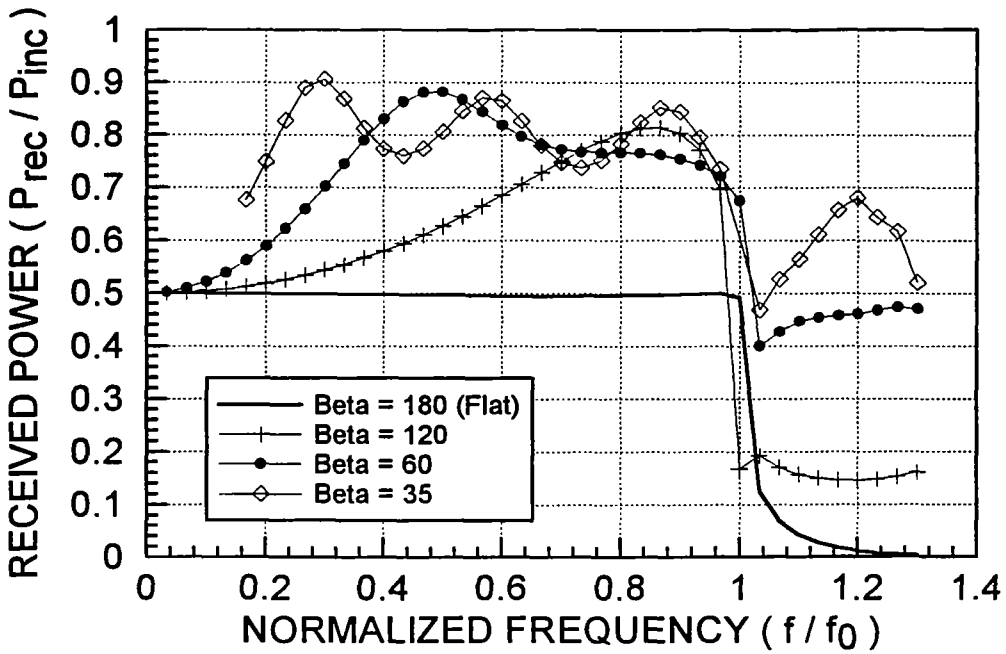

Figure 9. Frequency Response at Normal Incidence for Three TEM Horn Arrays and Planar Bicone Array

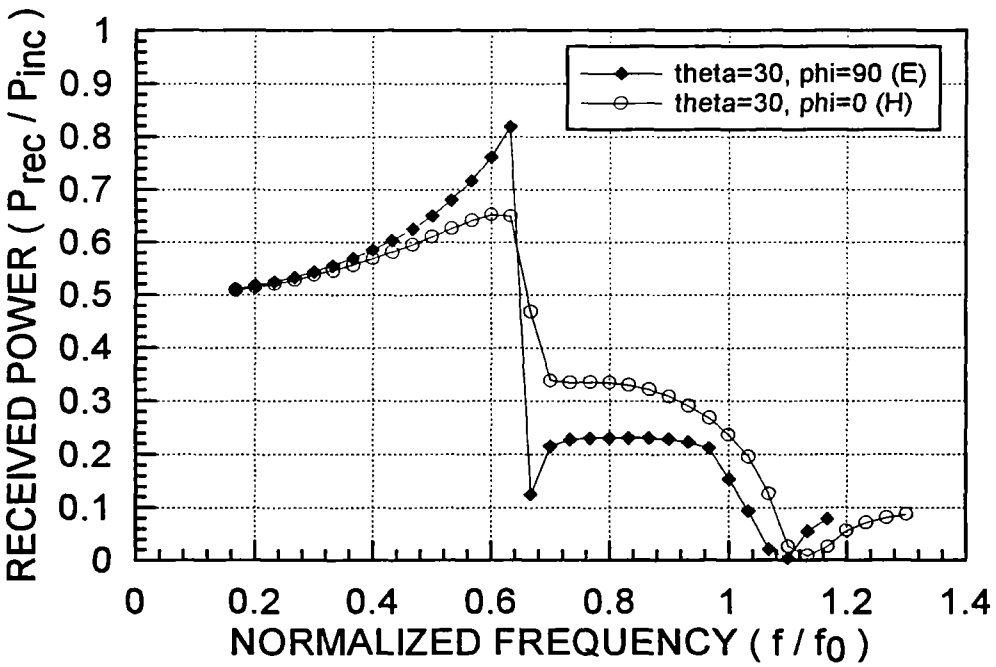

Figure 10. Frequency Response for β=120° TEM Horn Array at 30° Incidence in E and H Planes

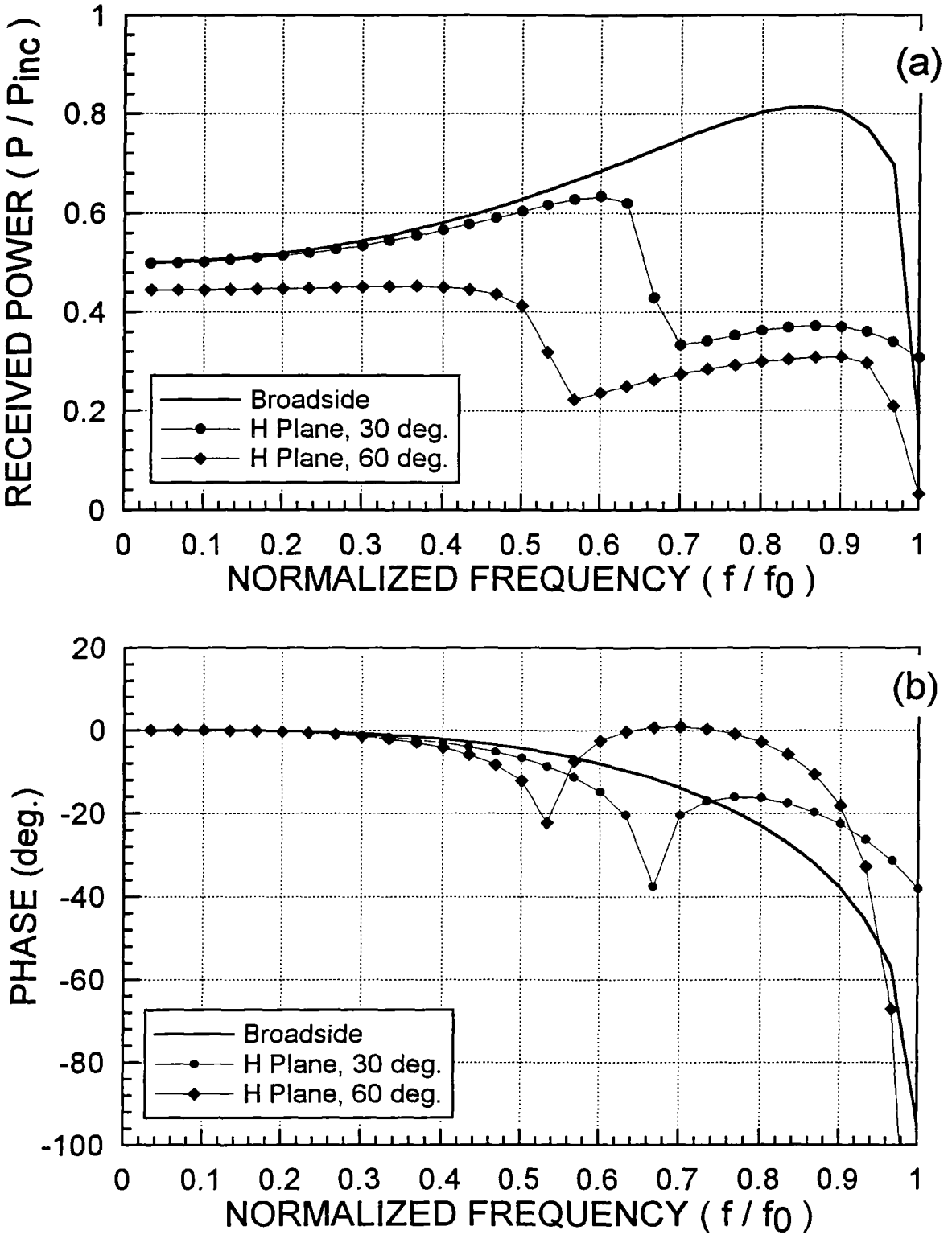

Figure 11. Received Power (top) and Phase (bottom) for β=120° TEM Horn Array, 0°, 30° and 60° Incidence (H Plane).

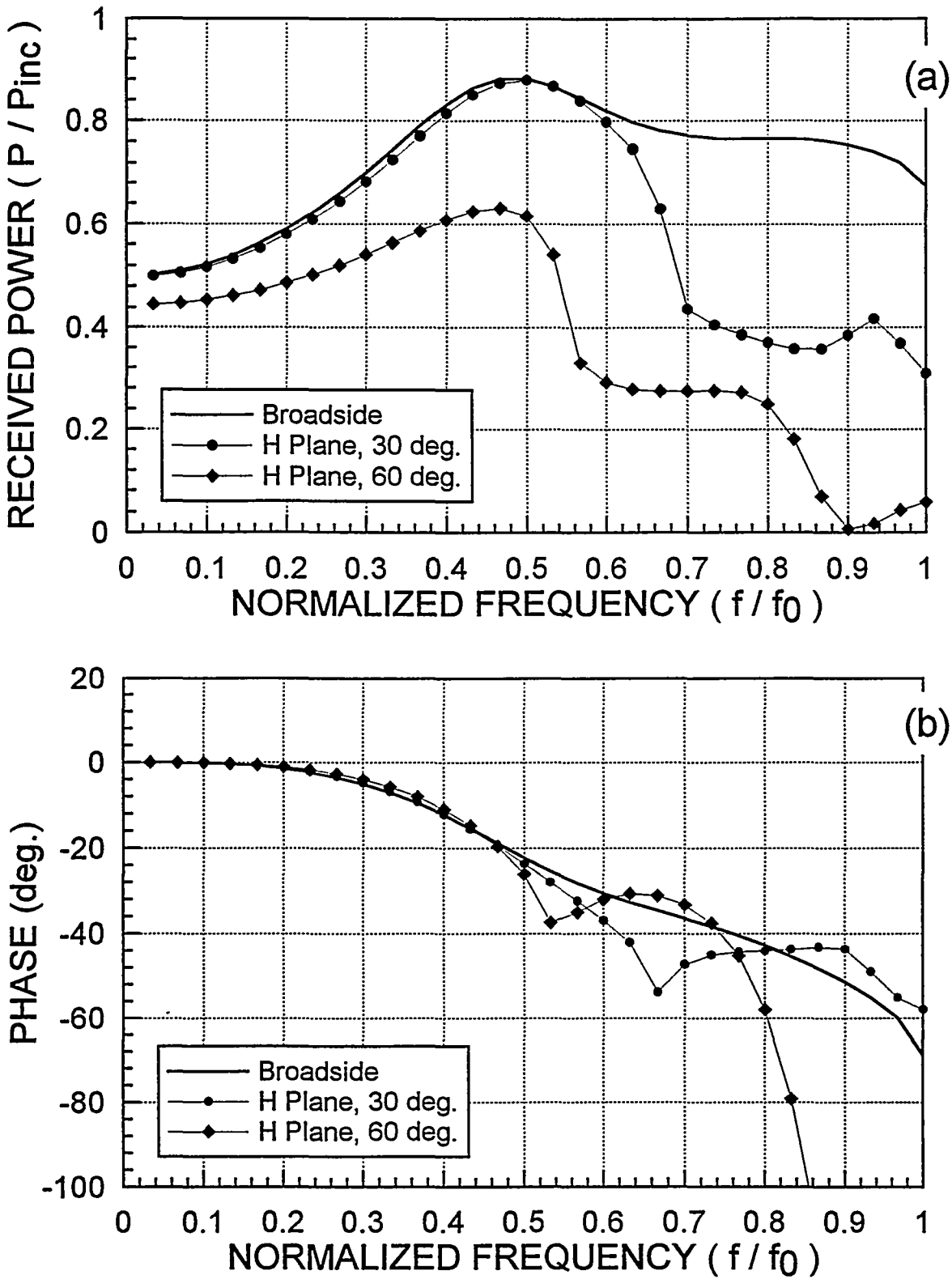

Figure 12. Received Power (top) and Phase (bottom) for β=60° TEM Horn Array, 0°, 30° and 60° Incidence (H Plane)

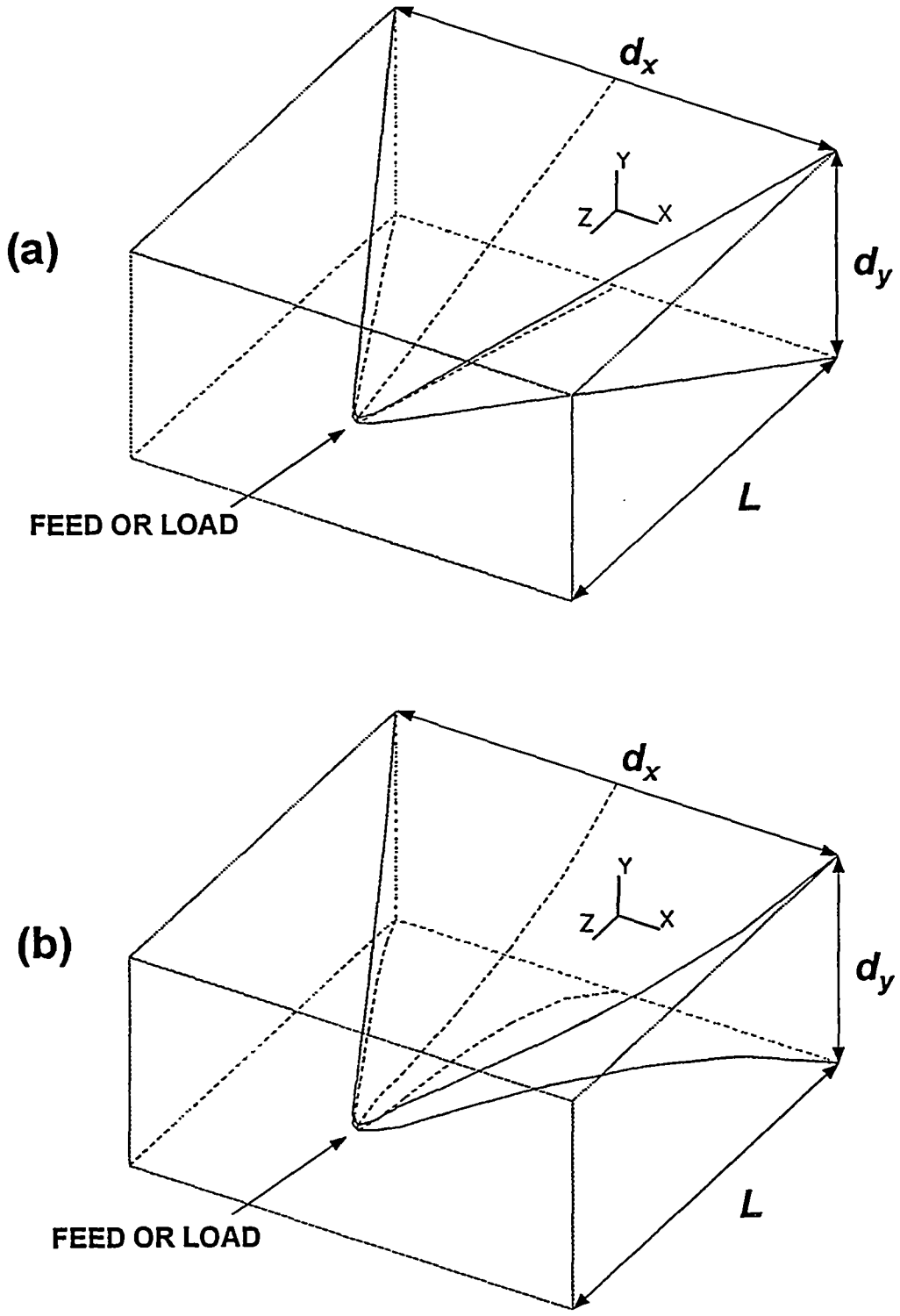

Figure 13. Linear and Exponential Flare TEM Horn Geometries with 2:1 Aperture Aspect Ratio

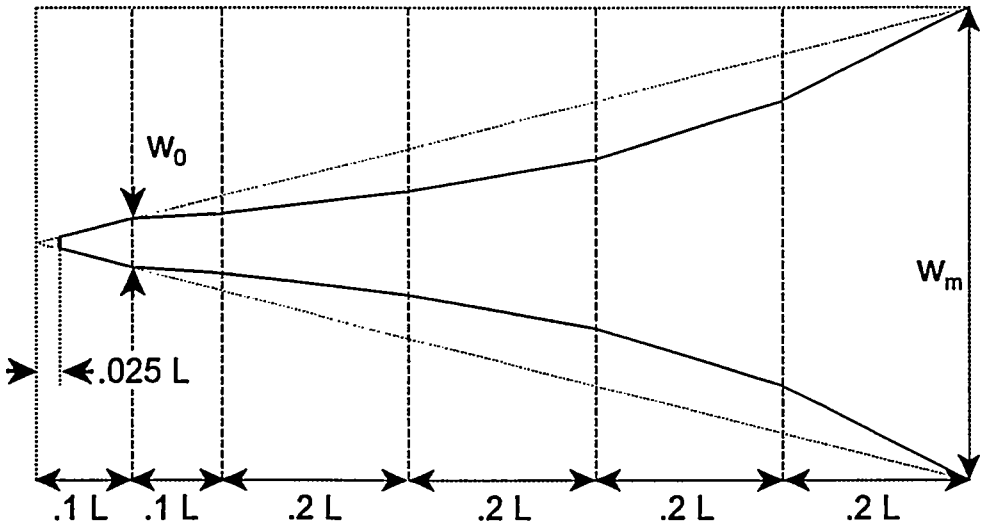

(a)

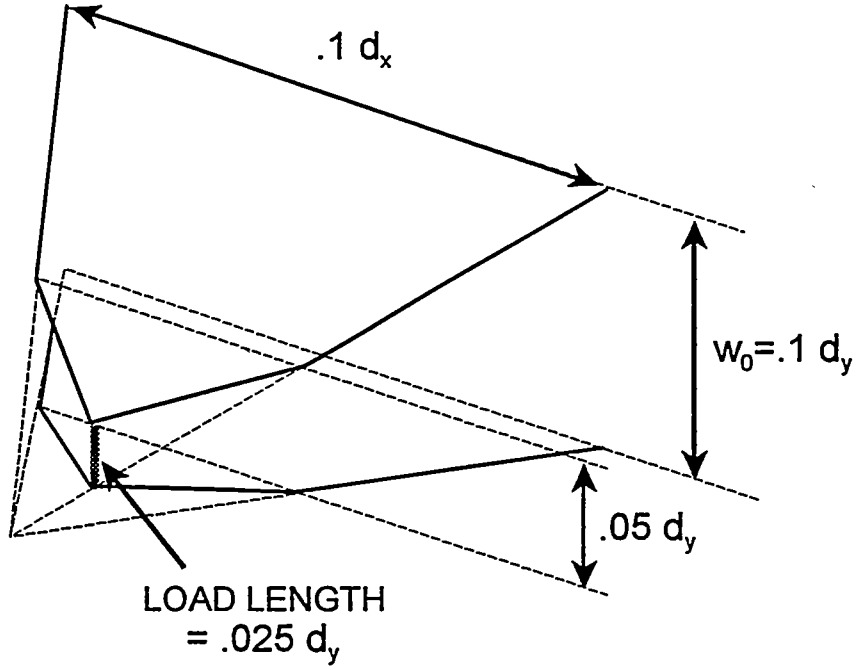

(b)

Figure 14. Flare and Feed Point Geometry for Exponential-flare Horn

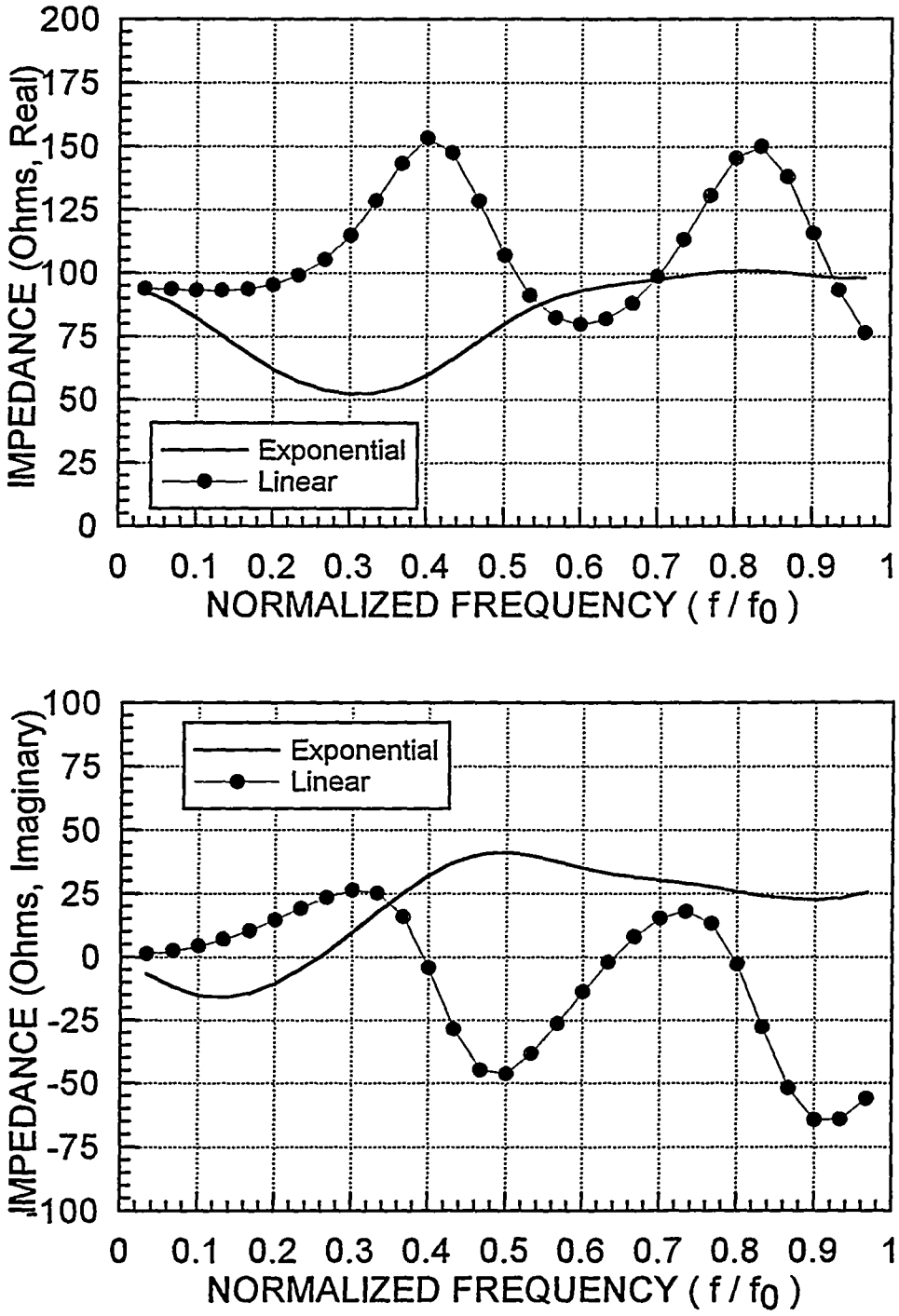

Figure 15. Input Impedance vs. Frequency Comparison for Linear- and Exponential-flare TEM Horns (open backed): (top) Real; (bottom) Imaginary

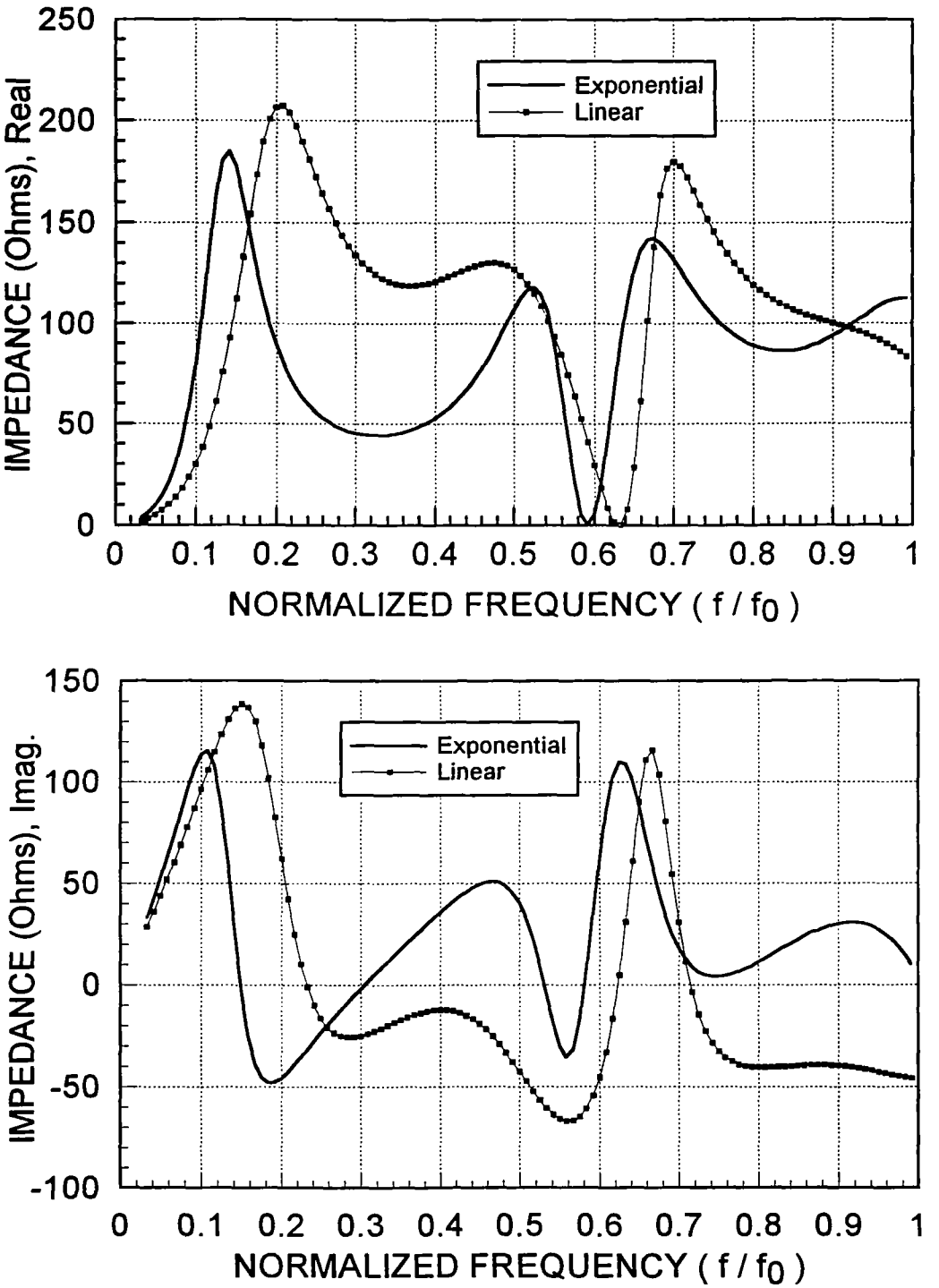

Figure 16. Input Impedance vs. Frequency Comparison for Linear- and Exponential-flare TEM Horns (ground plane-backed): (top) Real; (bottom) Imaginary

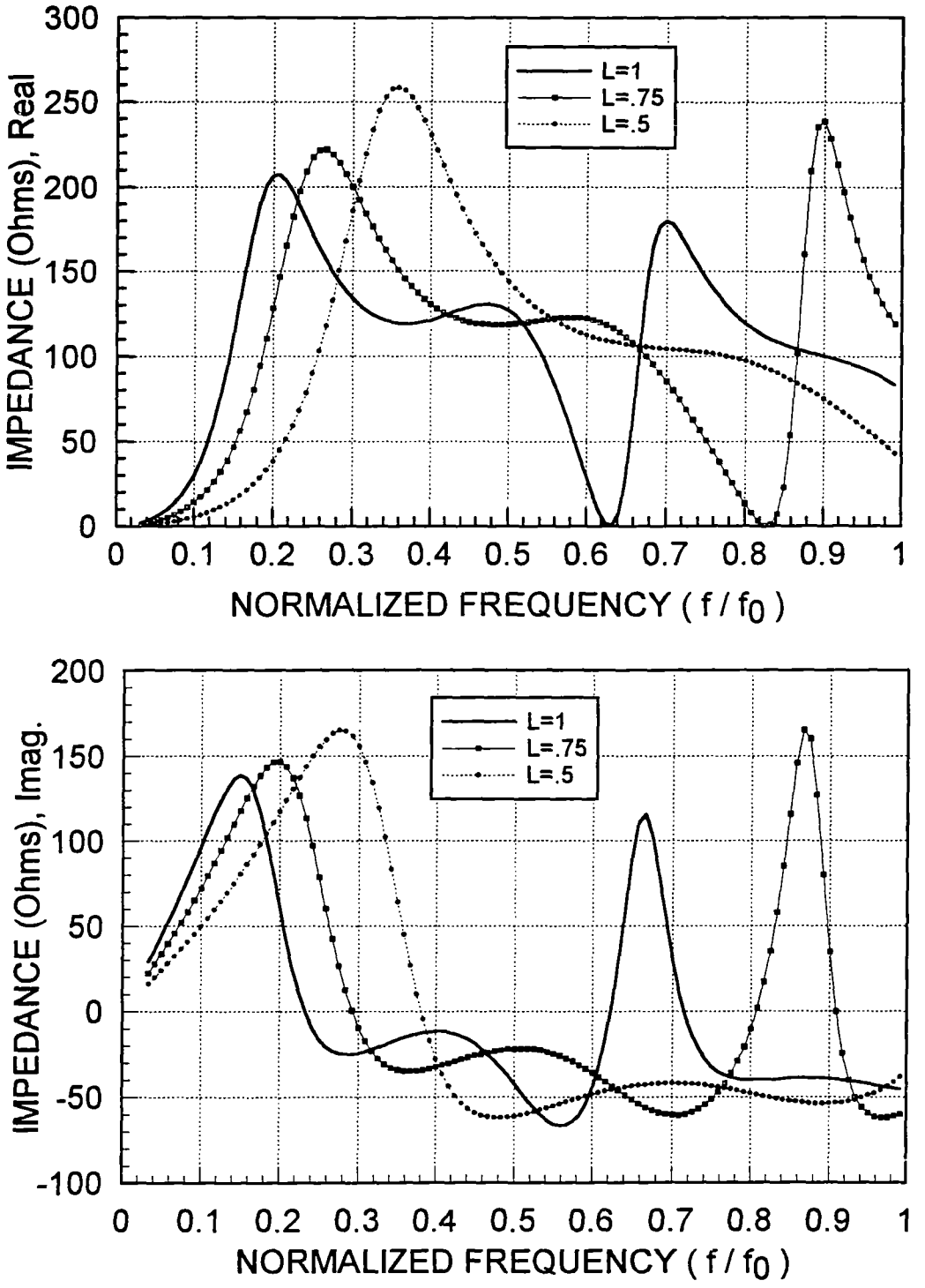

Figure 17. Input Impedance vs. Frequency for Ground Plane-backed Linear-flare TEM Horns with L/λ_0 = .5,.75 and 1.0: (top) Real; (bottom) Imaginary

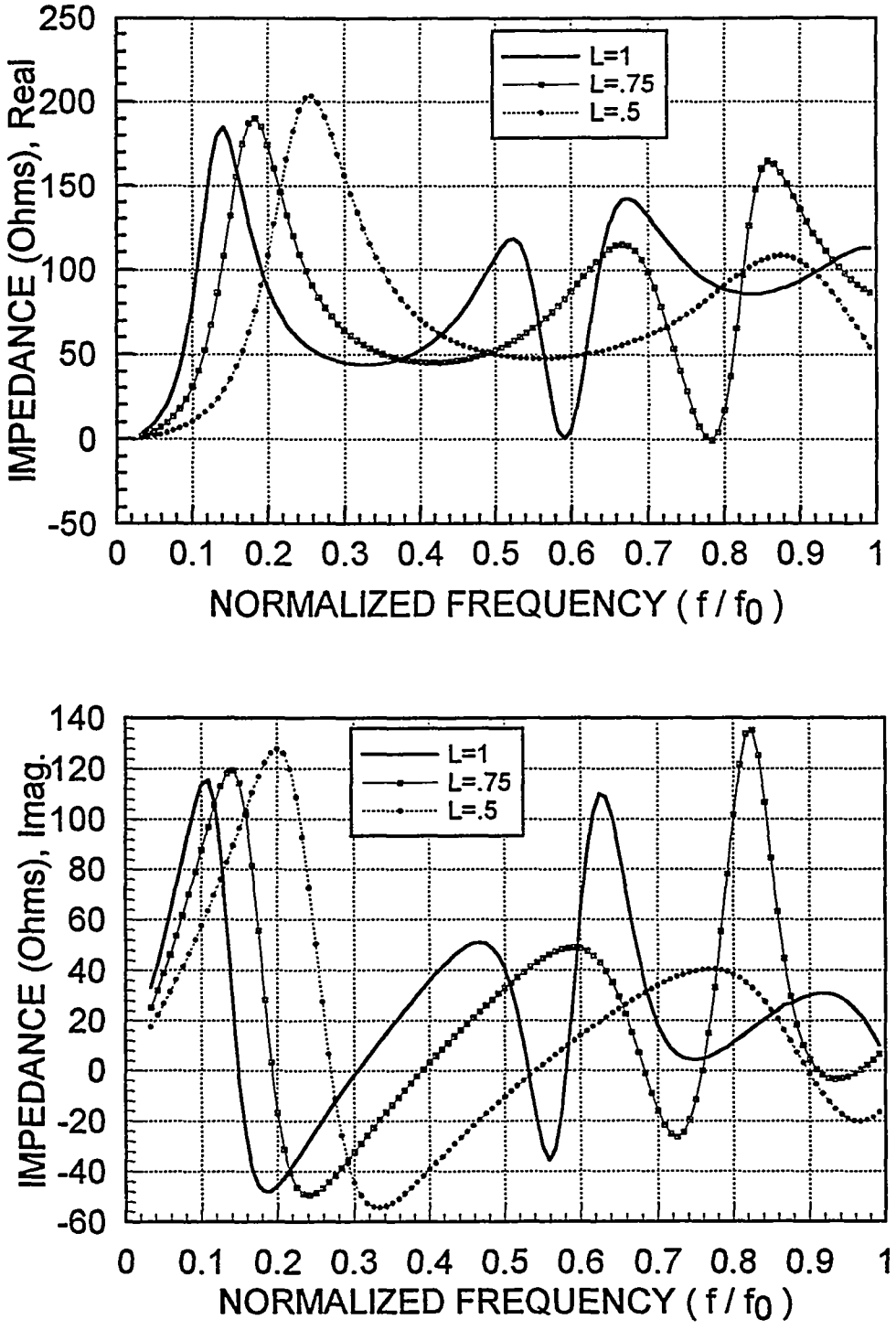

Figure 18. Input Impedance vs. Frequency for Ground Plane-backed Exponential-flare TEM Horns with L/λ_0 = .5,.75 and 1.0: (top) Real; (bottom) Imaginary

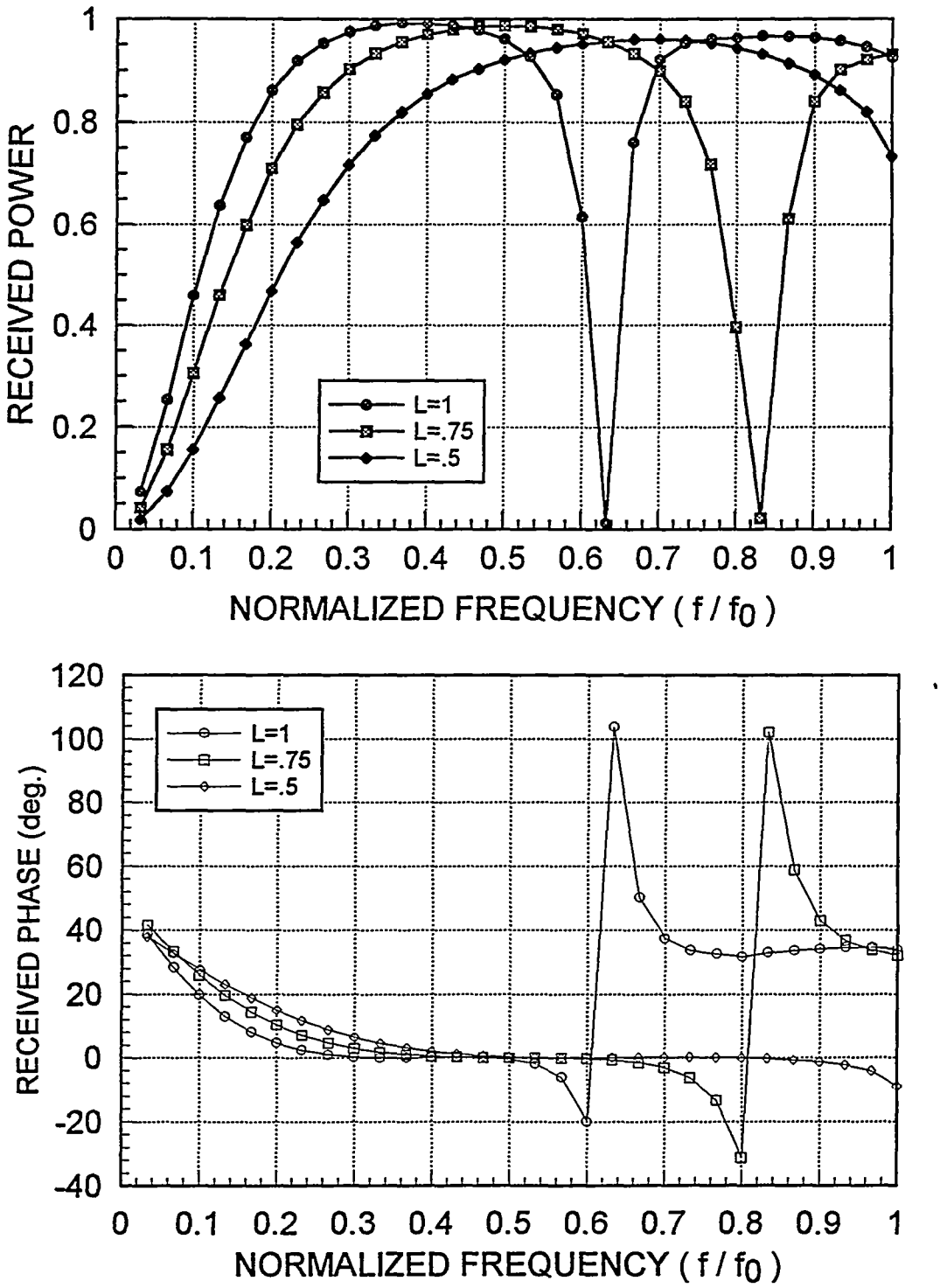

Figure 19. Frequency Response at Broadside Incidence for Ground Plane-backed Linear-flare TEM Horns with $L/\lambda_0 = .5, .75$ and 1.0:
(top) Received Power; (bottom) Phase

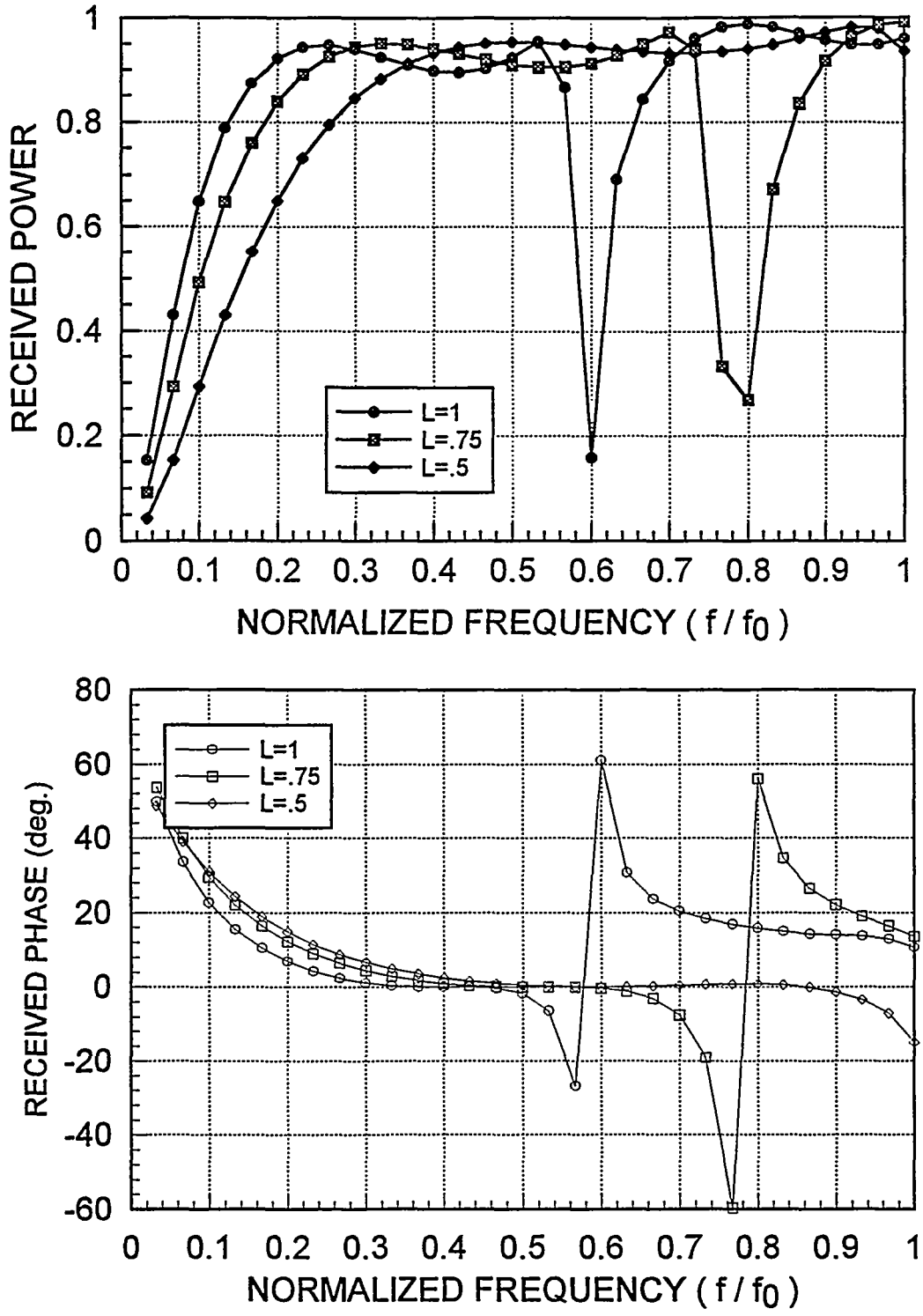

Figure 20. Frequency Response at Broadside Incidence for Ground Plane-backed Exponential-flare TEM Horns with $L/\lambda_0 = .5,.75$ and 1.0: (top) Received Power; (bottom) Phase

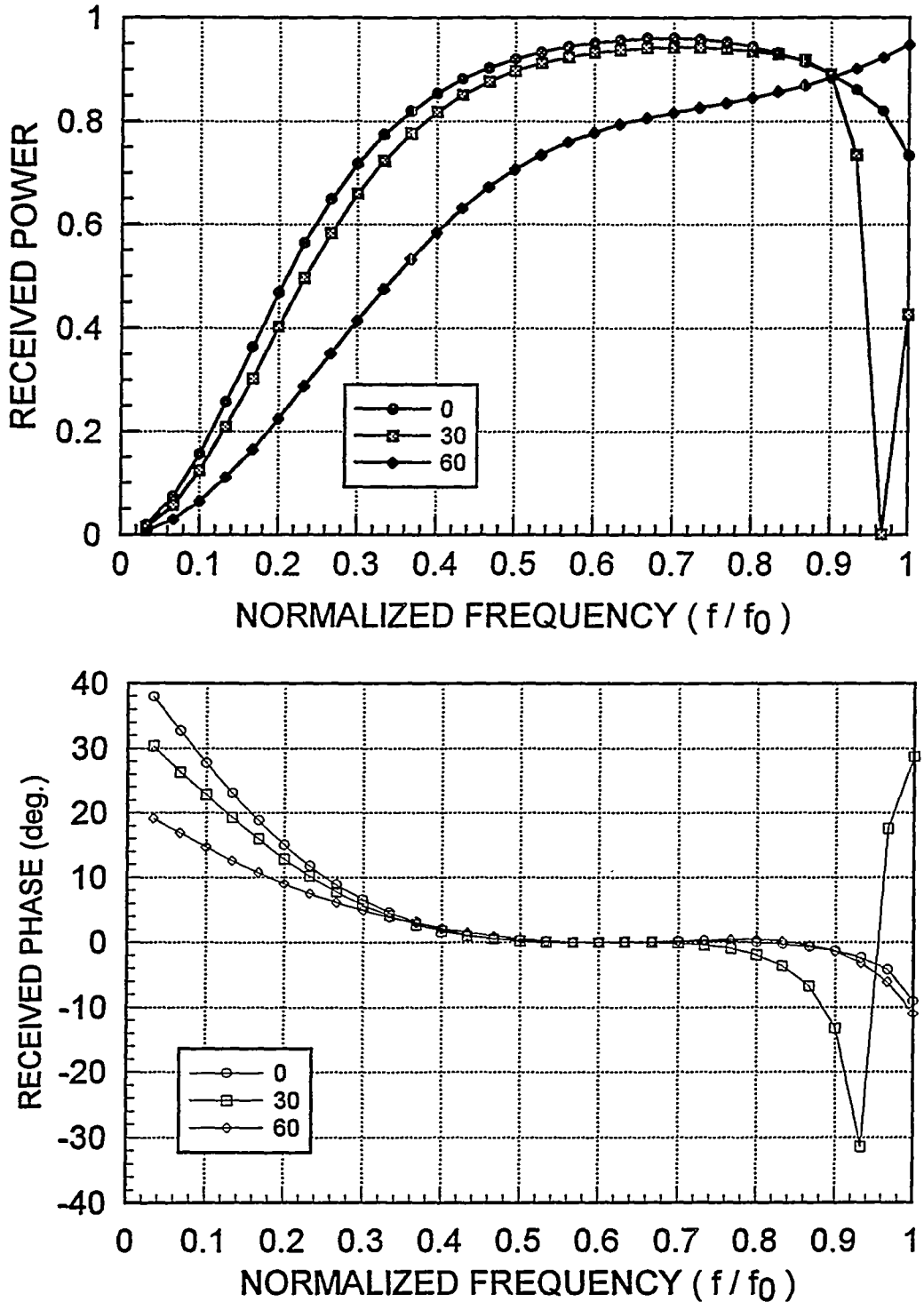

Figure 21. Frequency Response for Ground Plane-backed Linear-flare TEM Horns with $L/\lambda_0 = .5$, E Plane Scanning: (top) Power; (bottom) Phase

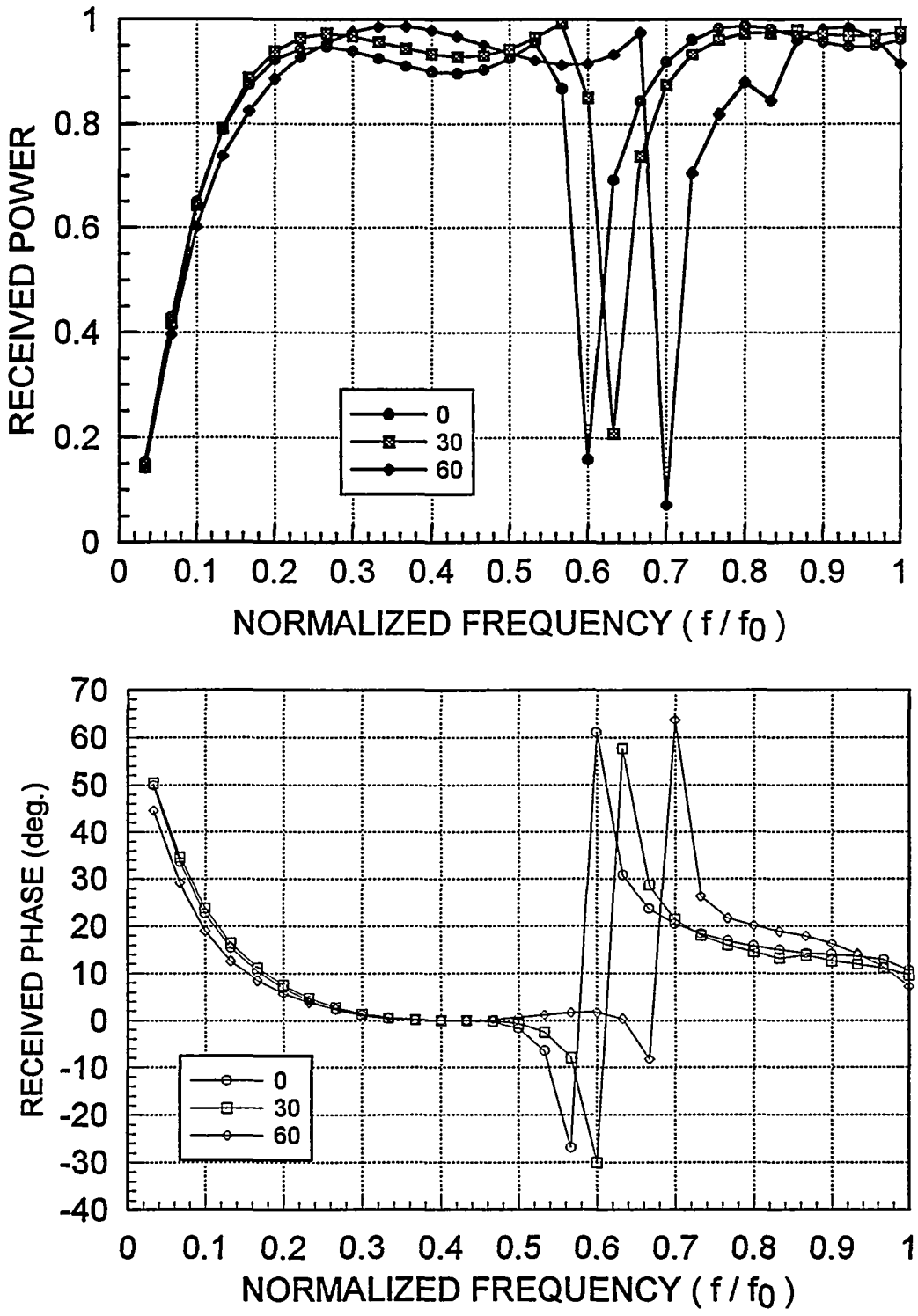

Figure 22. Frequency Response for Ground Plane-backed Exponential-flare TEM Horns with $L/\lambda_0 = .5$, E Plane Scanning: (top) Power; (bottom) Phase

REFERENCES

1. Baum, Carl E., "Some Characteristics of Planar Distributed Sources for Radiating Transient Pulses," Sensor and Simulation Note #100, Air Force Research Laboratory, Kirtland AFB, NM, Mar., 1970.

2. McGrath, Daniel T., "Numerical Analysis of Planar Bicone Arrays," Sensor and Simulation Note #100, Air Force Research Laboratory, Kirtland AFB, NM, Dec. 1996.

3. McGrath, Daniel T. and Carl E. Baum, "Scanning and Impedance Properties of TEM Horn Arrays for Transient Radiation," submitted to *IEEE Transactions on Antennas and Propagation.*

4. McGrath, Daniel T. and Vittal P. Pyati, "Phased Array Antenna Analysis with the Hybrid Finite Element Method," *IEEE Transactions on Antennas and Propagation*, **AP-42**, pp. 1625-1630, Dec. 1994.

5. McGrath, Daniel T. and Vittal P. Pyati, "Periodic Structure Analysis Using a Hybrid Finite Element Method," *Radio Science*, **31**, pp. 1173-1179, Sep.-Oct. 1996.

6. Sarkar, Tapan K., "On the Application of the Generalized Biconjugate Gradient Method," *Journal of Electromagnetic Waves and Applications*, **1**, pp. 223-242, 1987.

7. Deschamps, Georges A., "Properties of Complementary Multiterminal Planar Structures," *IRE Transactions on Antennas and Propagation*, **AP-7**, pp. S371-S378, Dec. 1959.

8. Inagaki, Naoki, Yasuhiro Isogai and Yasuto Mushiake, "Ichimatsu Moyou Antenna--Self-Complementary Antenna with Periodic Feeding Points," *IECE Transactions,* **62**, pp. 388-395, 1979.

9. Baum, Carl E., "Transient Arrays," *Ultra-wideband, Short-pulse Electromagnetics 3*, Ed. C. Baum et. al., New York: Plenum Press, 1997, pp. 129-138.

10. Yang, F.C. and K.S.H. Lee, "Impedance of Two-Conical Plate Transmission Line," Sensor and Simulation Note #221, Air Force Research Laboratory, Kirtland AFB, NM, Nov. 1976.

11. Amitay, Noach, Victor Galindo and Chen-Pang Wu, *Theory and Analysis of Phased Array Antennas*, Wiley-Interscience, 1972.

12. Choung, Y.H. and C.C. Chen, "44 GHz Slotline Phased Array Antenna," *Digest, 1989 IEEE Antennas and Propagation International Symposium*, pp. 1730-1733, Jun. 1989.

13. McGrath, Daniel T., "Blindness Effects in Ground Plane-Backed TEM Horn Arrays," to be published in: *Digest, 1998 IEEE Antennas and Propagation International Symposium*, Atlanta, GA, Jun. 1998.